Research Article

Enhanced Broad-Spectrum Protection Against High-Energy Visible Light Using Co-Doped Ag_2O and ZnO–TiO_2 Nanocomposites

Wittawat Ratanathavorn*, Nattaporn Boohuad and Rittipun Rungruang
Cosmetic Science Program, Faculty of Science and Technology, Suan Dusit University, Bangkok, Thailand

* Corresponding author. E-mail: wittawat_rat@dusit.ac.th DOI: 10.14416/j.asep.2025.09.009
Received: 4 June 2025; Revised: 4 July 2025; Accepted: 29 July 2025; Published online: 23 September 2025

Abstract
An Ag_2O-Zn/TiO_2 (AZT) nanocomposite was developed to overcome the limitations of conventional ZnO- and TiO_2-based sunscreens, which offer UV protection but lack efficacy against high-energy visible (HEV) light. The nanocomposite was synthesized using a sol–gel co–doping method, incorporating Ag_2O to enhance photocatalytic activity and enable plasmonic absorption in the HEV range. Its morphological structure and elemental composition were analyzed using field emission scanning electron microscopy (FE-SEM) with energy-dispersive X-ray spectroscopy (EDX). X-ray diffraction (XRD) was used to assess the crystalline structure, and optical properties were evaluated using a UV–visible spectrophotometer. The nanocomposite exhibited crystallite sizes ranging from 28.6 to 33.2 nm, with a predominant rutile phase. Optical properties revealed an energy bandgap ranging from 2.16 to 3.02 eV and broad-spectrum absorption extending into the HEV region (417–574 nm). The incorporation of Ag_2O improved HEV attenuation compared to conventional ZnO and TiO_2. *In vitro* SPF testing showed that Ag_2O-Zn/TiO_2 provided moderate UV protection, with values comparable to conventional TiO_2. Notably, it offered a more balanced UVA/UVB protection profile, highlighting its potential as an effective broad-spectrum UV filter.

Keywords: Co-doping method, High-energy visible light, Nanomaterials, Optical properties, Sol-gel method

1 Introduction

Solar radiation consists of approximately 49% infrared (IR) radiation, 43% visible light, and 5-8% ultraviolet (UV) radiation, though these values may vary due to atmospheric conditions and geographic location. Blue light (high-energy visible: HEV) is a part of the visible spectrum, with wavelengths ranging from 450 to 500 nm. It has higher energy and shorter wavelengths compared to other visible light colors [1]. Blue light is emitted not only by solar radiation but also by electronic devices such as smartphones, computers, tablets, TVs, fluorescent lights, and LED-based lighting. Blue light radiation penetrates deep into the skin, leading to the production of reactive oxygen species (ROS), which induce oxidative stress and cause damage to skin cells, proteins, and lipids, thereby accelerating the aging process. Additionally, blue light can trigger inflammatory responses, exacerbating conditions such as acne and rosacea [2], [3]. Studies also suggest that blue light can stimulate melanogenesis, leading to hyperpigmentation, particularly in individuals with darker skin tones [4]. Furthermore, blue light exposure may accelerate collagen degradation, contributing to the formation of wrinkles and fine lines, which are characteristics of photoaging. Finally, prolonged blue light exposure can impair the skin barrier function, increasing susceptibility to environmental damage and moisture loss [5], [6].

Conventional physical sunscreens, also known as mineral sunscreens, typically contain active ingredients such as ZnO and TiO_2, which physically block or reflect UV radiation. However, these materials are primarily designed to protect against UV-A and UV-B radiation, and their blue light shielding capacity remains limited due to insufficient absorption in the visible range.

TiO_2 is widely applied in UV filtration, photocatalysis, and solar cells due to its high stability, low cytotoxicity, and strong photocatalytic activity. Similarly, ZnO, with a 3.4 eV bandgap and high exciton binding energy (60 meV), offers excellent UV-blocking properties, optical transparency, and thermal stability. Despite these advantages, both TiO_2 and ZnO suffer from critical limitations: rapid electron–hole recombination lowers photocatalytic efficiency, and their microparticle forms scatter visible light strongly, leading to an undesirable whitening effect on the skin [7]–[13].

To address these issues, nanoparticulate forms of TiO_2 and ZnO have been adopted, reducing visible scattering and improving aesthetic appeal. Moreover, TiO_2 has been coupled with other semiconductors such as ZnO to suppress recombination and enhance photocatalytic activity. This coupling facilitates charge transfer by aligning conduction and valence band positions, thereby improving carrier separation. However, despite these advances, TiO_2/ZnO-based systems still exhibit weak absorption in the high-energy visible (HEV) region (400–500 nm), limiting their effectiveness for blue light protection.

Furthermore, increasing the concentration of these metal oxides to improve HEV light scattering often intensifies the whitening effect, compromising their cosmetic applicability. Thus, a more effective strategy is needed to extend visible light absorption without sacrificing transparency, particularly in the context of developing next-generation sunscreen formulations that address both UV and HEV exposure risks [14]–[20].

Recent studies on co-doped systems such as Ag/TiO_2 [21], Sr–ZnO [22], and Al/Ni–TiO_2 [23] have demonstrated improved photocatalytic activity, primarily in the UV region. In contrast, the Ag_2O–Zn/TiO_2 nanocomposite developed in this study was designed to extend absorption into the high-energy visible (HEV) range while maintaining cosmetic transparency.

Its structural, optical, and UV–visible shielding properties were systematically evaluated for potential sunscreen applications, with particular focus on HEV protection. The Ag_2O-Zn/TiO_2 nanocomposite was synthesized by co-doping titanium dioxide (TiO_2) with silver oxide (Ag_2O) and zinc oxide (ZnO). This design enhances charge separation efficiency, suppresses electron-hole recombination, and leverages surface plasmon resonance (SPR) to achieve efficient high-energy visible (HEV) light absorption within the 400–500 nm wavelength range while maintaining desirable cosmetic properties.

2 Materials and Methods

2.1 *Synthesis of Ag_2O-Zn/TiO_2 nanocomposite powders*

Ag_2O–Zn/TiO_2 nanocomposite powders were synthesized via a sol–gel co-doping method, following methodologies validated in recent studies of ZnO–TiO_2 composites. Zinc acetate dihydrate ($Zn(O_2CCH_3)_2 \cdot 2H_2O$, ≥99% purity, KEMAUS, Australia), titanium(IV) isopropoxide ($Ti(OCH(CH_3)_2)_4$, Sigma-Aldrich), and silver nitrate ($AgNO_3$, 99.9% purity, POCH, Poland) were used as precursors. The synthesis employed a 9:1 molar ratio of titanium isopropoxide to zinc acetate dihydrate, a proportion optimized in prior work to stabilize anatase–rutile TiO_2 phases and enhance interfacial charge transfer in ZnO–TiO_2 systems [24]–[26]. Silver nitrate concentrations were varied at 0%, 0.1%, 0.25%, and 0.5% to modulate plasmonic and defect-mediated optical properties. The molar concentrations of Ag and Zn precursors were calculated relative to the amount of titanium precursor. A titanium isopropoxide solution was prepared by dissolving the precursor in deionized water and ethanol, followed by 30 min of stirring. Separately, a nitric acid solution was prepared by mixing HNO_3 in deionized water, which was then slowly added to the titanium isopropoxide solution under vigorous stirring at 60 °C for 2 h. A solution containing zinc acetate dihydrate and silver nitrate dissolved in ethanol was introduced to the mixture, and the pH was adjusted to 3 using NaOH, followed by stirring at 60 °C for 2 h until a white sol-gel formed. The synthesized samples were washed with a 50% ethanol solution and collected via membrane filtration using a polycarbonate membrane (0.22 μm pore size). After drying overnight in a hot-air oven at 120 °C, the powders were calcined at 600 °C for 2 h, a temperature demonstrated to optimize crystallinity and photocatalytic activity in Ag_2O–Zn/TiO_2 hybrids.

2.2 *Characterization of Ag_2O-Zn/TiO_2 nanocomposite powders*

The crystalline structures of the synthesized nanocomposites were analyzed using X-ray diffraction (XRD; Bruker D8) with a Cu-Kα radiation source (λ = 1.54 Å). Diffractograms were recorded over a 2θ range of 20° to 80°. Field emission scanning

electron microscopy (FE-SEM; JEOL JSM-IT800), equipped with an energy-dispersive X-ray spectrometer (EDS), was used to examine morphology and average particle sizes. Particle size distributions were determined from FE-SEM images using ImageJ software. Optical band gaps were calculated via Tauc plot analysis derived from UV-visible spectrophotometry (PerkinElmer Lambda 950), with spectra recorded across 250–800 nm at a step size of 1.0 nm. Conventional ZnO- and TiO_2-based sunscreen formulations served as reference materials for UV absorbance comparisons. A 0.01% w/w dispersion of the synthesized nanocomposites in ethylene glycol was prepared by sonication for 30 minutes. *In vitro* sun protection efficacy (SPF) was evaluated for both the synthesized nanocomposites and conventional as ZnO and TiO_2 sunscreens. Polymethyl methacrylate (PMMA) plates (Helioscience, 5 cm × 5 cm, 5 µm roughness) were used as substrates. Samples (0.0325 g) were uniformly dispersed onto PMMA plates to achieve a film thickness of 1.2 mg/cm², followed by air-drying for 30 min under controlled conditions (25 °C, 50% relative humidity). UV transmittance measurements were performed using a Labsphere UV-2000 Ultraviolet Transmittance Analyzer, spanning 250–450 nm with 1 nm resolution. Absorbance spectra were recorded in triplicate for statistical reliability.

3 Results and Discussion

3.1 *Physical appearance and characterization*

A high-energy visible light-protective compound was developed for cosmetic sunscreen applications, utilizing titanium dioxide (TiO_2) as the primary physical UV filter. To achieve this, the targeted material was required to be a fine, white powder devoid of any gray or black impurities. The inclusion of Ag_2O was found to influence the physical characteristics of the powder, with higher concentrations leading to a grayish-white appearance due to the formation of silver oxide clusters. Consequently, the proportion of Ag_2O was carefully controlled and maintained below 0.5% of the nanocomposite to ensure a predominantly white appearance. This precise regulation allowed the material to retain desirable cosmetic properties while providing effective blue light blocking and UV protection (Figure 1).

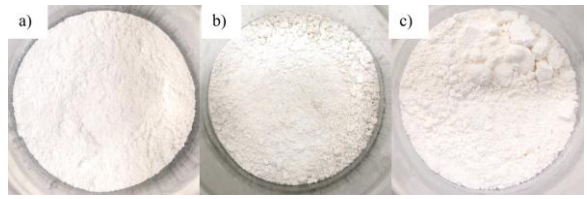

Figure 1: Physical appearance of the synthesized Ag_2O-Zn/TiO_2 nanocomposite in: (a) 0.1% Ag_2O-Zn/TiO_2; (b) 0.25% Ag_2O-Zn/TiO_2; and (c) 0.5% Ag_2O-Zn/TiO_2.

The FE-SEM images (Figure 2(a)–(d)) confirmed nanocrystalline morphology and revealed increased particle size with higher Ag_2O content. This trend was attributed to silver nanoparticles promoting aggregation and growth. The observed size dependence suggested that Ag nanoparticles acted as nucleation sites, facilitating controlled growth and selective aggregation during synthesis. Complementary EDS mapping (Figure 2(e)–(h)) confirmed the presence and distribution of Zn and Ag throughout the TiO_2 matrix, as indicated by characteristic emission peaks. The uniform elemental dispersion indicated effective doping with minimal phase segregation. The uniform distribution of these elements suggested that effective doping had been achieved with minimal phase segregation. The powder XRD analysis (Figure 3) was conducted and revealed a complex phase composition in the synthesized nanocomposites, attributed to competing phase stabilization mechanisms and multicomponent interactions. The rutile phase was predominantly observed in TiO_2, as indicated by strong diffraction peaks at $2\theta = 27.28°$ (110), 35.95° (101), and 40.88° (111), matching the standard rutile pattern (JCPDS 88-1175). A minor anatase phase was identified by a broadened peak at $2\theta = 25.32°$ (101), resulting from incomplete phase transformation under the subcritical calcination temperature (600 °C). At this temperature, a kinetic barrier inhibited the anatase-to-rutile transition, as the thermodynamic driving force becomes significant only above 700 °C [27].

Nanoscale crystallites were confirmed by the broadened anatase peak, indicating restricted growth at lower temperatures. Ag_2O phases were clearly detected at $2\theta = 32.52°$ (111) and 37.58° (021), while the absence of ZnO signals suggested that Zn^{2+} ions were incorporated into the TiO_2 lattice via interstitial or substitutional mechanisms. This was further supported by a 0.15° shift in rutile peaks toward lower angles in undoped ZT composites, indicating lattice expansion due to Zn^{2+} incorporation (ionic radius 0.74 Å vs. Ti^{4+} 0.605 Å) [28].

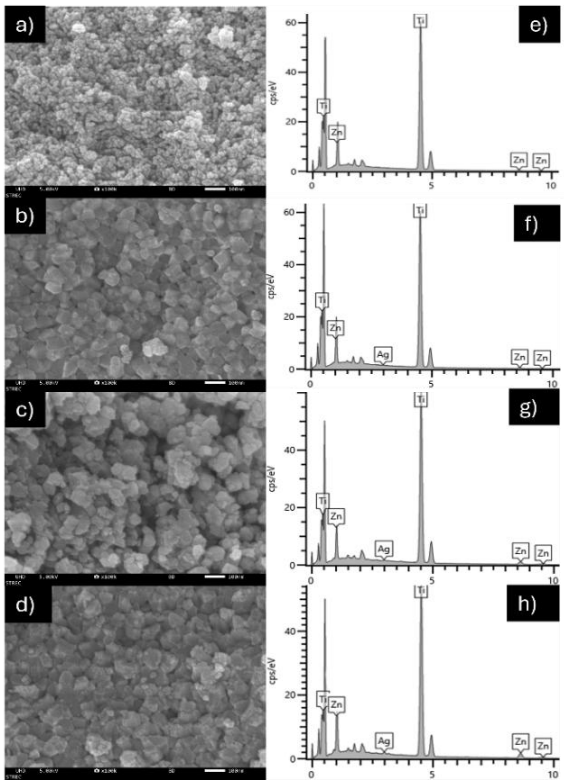

Figure 2: FE-SEM images demonstrate that the morphologies of Ag_2O-Zn/TiO_2 nanocomposites in: (a) undoped ZT; (b) 0.1% Ag_2O-Zn/TiO_2; (c) 0.25% Ag_2O-Zn/TiO_2; and (d) 0.5% Ag_2O-Zn/TiO_2. Energy dispersive X-ray spectroscopy (EDS) pattern of (e) undoped ZT; (f) 0.1% Ag_2O-Zn/TiO_2; (g) 0.25% Ag_2O-Zn/TiO_2; and (h) 0.5% Ag_2O-Zn/TiO_2.

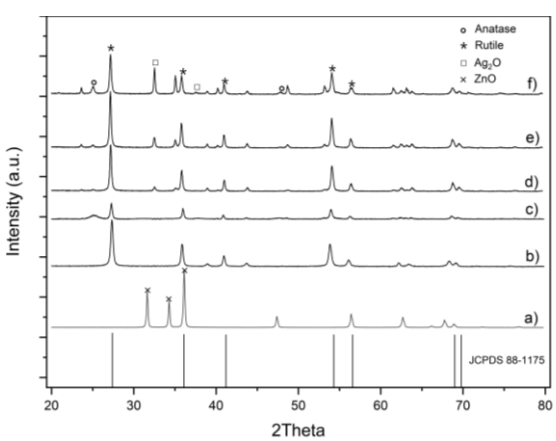

Figure 3: Powder X-ray diffraction (XRD) of (a) commercial ZnO; (b) commercial TiO_2; (c) ZT; (d) 0.10% Ag_2O-Zn/TiO_2; (e) 0.25% Ag_2O-Zn/TiO_2; and (f) 0.5% Ag_2O-Zn/TiO_2.

Table 1: Average particle sizes, crystal structures, and optical band gaps of the synthesized Ag_2O-Zn/TiO_2 nanocomposites.

Property		0.0% AZT	0.1% AZT	0.25% AZT	0.5% AZT	TiO_2	ZnO
Atomic %	Ti (K)	92.1	90.3	92.4	87.7	–	–
	Zn (K)	7.9	9.63	7.38	11.8	–	–
	Ag (K)	–	0.10	0.18	0.51	–	–
Crystal Size (nm)	TiO_2	30.7	30.8	30.3	30.1	27.7	–
	ZnO	–	–	–	–	–	48.9
	Ag_2O	–	28.6	30.9	33.2	–	–
Optical Bandgap (eV)		2.58	2.55	2.41	2.01	3.30	3.18
Critical Wavelength (nm)		482	486	515	617	376	390

In contrast, no detectable lattice parameter changes were exhibited by Ag_2O-doped composites, implying surface segregation of Ag species at grain boundaries. A progressive increase in crystallite size with Ag doping (28.6 nm in undoped ZT to 33.2 nm in 0.5% Ag_2O-Zn/TiO_2), as shown in Table 1, was revealed by Scherrer analysis, attributed to heterogeneous growth of TiO_2 and ZnO domains promoted by Ag_2O clusters acting as nucleation sites. This agglomeration-driven growth was corroborated by rising XRD signal-to-noise ratios, reflecting improved crystallinity and reduced lattice strain.

3.2 *UV–visible absorbance of the Ag_2O-Zn/TiO_2 nanocomposite*

The UV–visible absorbance spectra of the synthesized Ag_2O-Zn/TiO_2 (ZT) nanocomposites were compared to conventional TiO_2- and ZnO-based sunscreens (Figure 4). Bandgap energies (*Eg*) were calculated using the Tauc relation for direct semiconductors (Equation (1)), [29], [30].

$$\alpha = K(h\nu - E_g)^n / h \quad (1)$$

Where α represents the absorption coefficient, K is a constant related to the properties of the material, $h\nu$ denotes the energy of the photon, n is an exponent that depends on the nature of the bandgap, and E_g is the bandgap energy. The bandgap energies were determined by constructing a Tauc plot, in which $(\alpha h\nu)^2$ was plotted against hv, and extrapolated to the x-axis at α = 0.

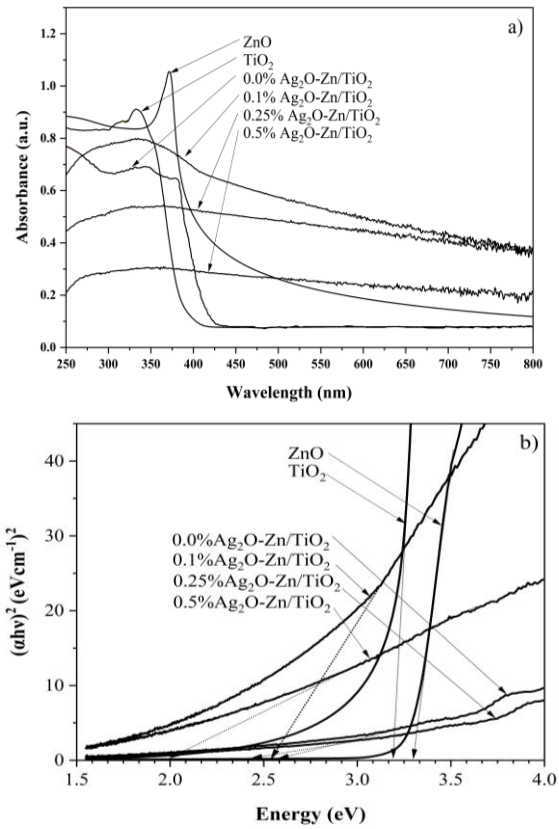

Figure 4: (a) UV-vis spectra of conventional sunscreens and the synthesized Ag_2O-Zn/TiO_2 nanocomposite. (b) Tauc plots constructed for optical bandgap determination.

The results indicated that conventional sunscreens containing nano-TiO_2 and nano-ZnO primarily absorbed light in the UV region (250–400 nm), with characteristic absorption peaks at approximately 388 nm and 375 nm, respectively. TiO_2 exhibited strong absorption in the UVB region (320–380 nm), while ZnO showed greater emphasis on UVA protection (315–400 nm). However, a significant drop in absorption intensity was observed across the visible spectrum (400–500 nm), highlighting the limited efficiency of these materials in shielding high-energy visible (HEV) light [31], [32].

In contrast, undoped ZnO–TiO_2 composites (0.0% Ag_2O–Zn/TiO_2) were found to extend the absorption edge to 410 nm, while maintaining UV-dominant absorption due to the wide band gaps of the individual components (ZnO: 3.31 eV; TiO_2: 3.20 eV) [33]. The bandgap narrowing to 3.02 eV in the undoped composite was attributed to Zn^{2+} substitution within the TiO_2 lattice, resulting in the formation of oxygen vacancies and localized mid-gap states. These electronic modifications lowered the Fermi level, reduced the bandgap, and induced a redshift in the absorption edge. In addition to the Tauc analysis, the increase in Urbach energy and noticeable absorption tailing in Ag-doped samples indicate the formation of mid-gap states, which contribute to enhanced sub-bandgap absorption and improved light-harvesting efficiency [34].

This limitation was further addressed through Ag_2O doping, whereby intermediate energy states were introduced via the 4d orbitals of Ag^+ and oxygen vacancies (VO^{2-}), reducing the bandgap to 2.16–2.58 eV. Additionally, synergistic heterojunction effects between ZnO and TiO_2 enhanced charge separation, while the interaction between Ag and the TiO_2–ZnO matrix promoted efficient electron transfer, collectively improving HEV light absorption performance.

Furthermore, efficient charge transfer was facilitated by the interaction between the Ag d-orbitals and the conduction band of ZnO–TiO_2, which reduced recombination losses. Although no distinct ZnO diffraction peaks were detected by XRD, the enhanced charge separation behavior strongly supports the formation of localized ZnO-like domains or subphases at the TiO_2 interface, which may not be sufficiently crystalline or concentrated to generate separate diffraction signals. This is consistent with previous studies reporting that Zn^{2+} can be partially substituted into the TiO_2 lattice while concurrently forming interfacial heterojunctions at the nanoscale [22], [23], [35], [36]. This modification led to a broad-spectrum absorption range (250–650 nm), extending coverage into the HEV range [37].

The optical band gaps of conventional sunscreens containing nano-ZnO and nano-TiO_2 were determined to be 3.31 eV and 3.20 eV, respectively. The bandgap energies of the synthesized undoped and doped Ag_2O-Zn/TiO_2 nanocomposites were measured as 3.02 eV (0.0%Ag_2O-Zn/TiO_2), 2.58 eV (0.1%Ag_2O-Zn/TiO_2), 2.47 eV (0.25%Ag_2O-Zn/TiO_2), and 2.16 eV (0.5%Ag_2O-Zn/TiO_2). These values corresponded to absorption wavelengths in the blue-light region at 410 nm, 480 nm, 502 nm, and 574 nm, respectively, indicating a significant redshift in optical activity with increasing Ag_2O doping. The reduction in bandgap for the undoped ZT composites was attributed to the incorporation of Zn^{2+} into the TiO_2 lattice, which altered the electronic structure of the material. Further reduction in the band gap with Ag_2O doping was explained by the introduction of intermediate energy states within the ZnO–TiO_2 bandgap,

resulting from the incorporation of Ag. These intermediate states, associated with Ag^+ ions and oxygen vacancies, significantly modified the electronic structure and enhanced absorption in the visible light range. This synergistic modification led to a significant enhancement of visible-light activity, making the Ag_2O-Zn/TiO_2 nanocomposites highly effective for applications requiring blue-light protection, such as transparent sunscreens, digital screen filters, and photocatalytic systems that relied on panchromatic responsiveness. The optimal performance was achieved with 0.1%Ag_2O-Zn/TiO_2, which exhibited absorption wavelengths in the blue-light region (450–490 nm) and enhanced photocatalytic activity. It was found that higher doping levels (>0.25% Ag_2O) resulted in the formation of metallic Ag clusters, which acted as recombination centers, reducing charge separation efficiency and quantum yield, and thus decreasing absorption activity [38]. These properties made Ag_2O-Zn/TiO_2 composites highly promising for advanced applications in blue-light screening technologies and environmental remediation [39]–[43].

3.3 *Evaluation of sun protection efficiency*

The *in vitro* SPF testing results are shown in Table 2. Differences in UV protection efficiency and UVA/UVB balance were evaluated using SPF, UVAPF, SPF/UVAPF ratio, and UVA/UVB values. SPF values of 9.27, 11.5, and 8.32 were measured for 0.1% Ag_2O/ZT, TiO_2, and ZnO, respectively. TiO_2 showed the highest SPF (11.5) and UVAPF (10.79), due to its high refractive index and strong UVB scattering [42]. Ag_2O/ZT exhibited moderate SPF (9.27) and UVAPF (8.79), while ZnO showed the lowest SPF (8.32) but a relatively high UVAPF (8.74), confirming its known UVA attenuation capability [44], [45].

Table 2: The SPF, UVAPF, SPF/UVAPF ratio, and UVA/UVB values for the tested samples.

Samples	SPF	UVAPF	SPF/UVAPF	UVA/UVB
0.1%Ag_2O-Zn/TiO_2	9.27	8.79	1.054	0.992
TiO_2	11.5	10.79	1.065	0.932
ZnO	8.32	8.74	0.952	0.957

The SPF/UVAPF ratio was used to assess the uniformity of UV protection. Values near 1 were found for Ag_2O-Zn/TiO_2 (1.054) and TiO_2 (1.065), indicating balanced UVA/UVB protection. ZnO's lower ratio (0.952) reflected its stronger UVA preference [29]. Given the focus on UVA protection in modern sunscreens, ZnO's performance was considered beneficial for reducing oxidative stress and photoaging [46].

The UVA/UVB ratio was analyzed to characterize spectral balance. TiO_2 showed the lowest value (0.932), indicating stronger UVB absorption, while Ag_2O-Zn/TiO_2 displayed the highest (0.992), providing the most balanced protection. ZnO's ratio (0.957) was slightly lower, showing a UVA-biased response [20], [47].

Notably, many commercial mineral-based sunscreens typically show UVA/UVB ratios in the range of 0.8–0.95, with a focus on UVB protection. In comparison, the Ag_2O-Zn/TiO_2 nanocomposite offers more uniform spectral attenuation, indicating its strong potential for use in broad-spectrum formulations that address both short-term UVB effects and long-term UVA-induced skin damage.

4 Conclusions

In this study, Ag_2O-Zn/TiO_2 nanocomposites were successfully synthesized via sol-gel co-doping. Ag_2O doping introduced impurity levels and oxygen vacancies, narrowing the optical bandgap from 3.02 to 2.16 eV and enhancing blue-light absorption (410–574 nm). The 0.1% Ag_2O-Zn/TiO_2 sample showed the best photocatalytic activity under visible light due to improved electron-hole separation. The composites also demonstrated strong potential as sunscreen agents, achieving a high UVA/UVB ratio of 0.992 and an SPF of 9.27. Compared to conventional TiO_2 and ZnO, the Ag_2O-doped materials offered more balanced UV protection and effective HEV light shielding, making them promising for broad-spectrum sunscreen applications. Future investigations will include compatibility testing with sunscreen formulations, clinical evaluation of sun protection efficacy, and stability testing of sunscreen products to confirm the suitability of the nanocomposites for sunscreen applications.

Acknowledgments

We would like to express our sincere gratitude to the Research and Development Institute at Suan Dusit University for their generous financial support (Fundamental Fund: 2023) [grant numbers FF67-193085]. We also acknowledge the Cosmetic Science Program, Faculty of Science and Technology, Suan Dusit University, for providing the necessary equipment for this research.

Author Contributions

W.R.: conceptualization, formal analysis, funding acquisition, methodology, validation, writing – original draft, writing – review & editing; R.R.: data curation, formal analysis, resources, visualization; N.B.: formal analysis, resources, validation. All authors have read and agreed to the published version of the manuscript.

Conflicts of Interest

The authors declare no conflict of interest.

References

[1] X. Zhang and X. Zhao, "The impact of blue light exposure on public health and protective strategies," *Current Research in Medical Sciences*, vol. 3, pp. 60–66, 2024, doi: 10.56397/CRMS.2024.06.08.

[2] H. W. Lim, I. Kohli, E. Ruvolo, L. Kolbe, and I. H. Hamzavi, "Impact of visible light on skin health: The role of antioxidants and free radical quenchers in skin protection," *Journal of the American Academy of Dermatology*, vol. 86, no. 3S, pp. S27–S37, Mar. 2022, doi: 10.1016/j.jaad.2021.12.024.

[3] F. Liebel, S. Kaur, E. Ruvolo, N. Kollias, and M. D. Southall, "Irradiation of skin with visible light induces reactive oxygen species and matrix-degrading enzymes," *Journal of Investigative Dermatology*, vol. 132, no. 7, pp. 1901–1907, Jul. 2012, doi: 10.1038/jid.2011.476.

[4] C. Regazzetti et al., "Melanocytes sense blue light and regulate pigmentation through Opsin-3," *Journal of Investigative Dermatology*, vol. 138, no. 1, pp. 171–178, Jan. 2018, doi: 10.1016/j.jid.2017.07.833.

[5] R. Campiche et al., "Pigmentation effects of blue light irradiation on skin and how to protect against them," *International Journal of Cosmetic Science*, vol. 42, no. 4, pp. 399–406, Aug. 2020, doi: 10.1111/ics.12637.

[6] S. J. Cooper and G. T. Bowden, "Ultraviolet B regulation of transcription factor families: Roles of nuclear factor-kappa B (NF-κB) and activator protein-1 (AP-1) in UVB-induced skin carcinogenesis," *Current Cancer Drug Targets*, vol. 7, pp. 325–334, 2007, doi: 10.2174/156800907780809714.

[7] J. Cihlar Jr., E. Bartonickova, and J. Cihlar, "Low-temperature sol–gel synthesis of anatase nanoparticles modified by Au, Pd and Pt and activity of TiO_2/Au, Pd, Pt photocatalysts in water splitting," *Journal of Sol-Gel Science and Technology*, vol. 65, pp. 430–442, 2013, doi: 10.1007/s10971-012-2955-8.

[8] J. Cihlar, V. Kasparek, M. Kralova, and K. Castkova, "Biphasic anatase-brookite nanoparticles prepared by sol–gel complex synthesis and their photocatalytic activity in hydrogen production," *International Journal of Hydrogen Energy*, vol. 40, pp. 2950–2962, 2015, doi: 10.1016/j.ijhydene.2015.01.008.

[9] M. C. Ceballos-Chuc, C. M. Ramos-Castillo, J. J. Alvarado-Gil, G. Oskam, and G. Rodríguez-Gattorno, "Influence of brookite impurities on the Raman spectrum of TiO_2 anatase nanocrystals," *Journal of Physical Chemistry C*, vol. 122, pp. 19921–19930, 2018, doi: 10.1021/acs.jpcc.8b04987.

[10] M. H. Yang et al., "Anatase and brookite TiO_2 with various morphologies and their proposed building block," *CrystEngComm*, vol. 16, pp. 441–447, 2014, doi: 10.1039/c3ce41750f.

[11] S. Rakhimkulov et al., "Synthesis and application of zinc oxide nanoparticles," *Research Journal of Chemistry and Environment*, vol. 28, pp. 947–966, 2024.

[12] N. Sedefoglu, "Characterization and photocatalytic activity of ZnO nanoparticles by green synthesis method," *Optik*, vol. 288, p. 171217, 2023, doi: 10.1016/j.ijleo.2023.171217.

[13] D. K. Sharma, S. Shukla, K. K. Sharma, and V. Kumar, "A review on ZnO: Fundamental properties and applications," *Materials Today: Proceedings*, vol. 49, pp. 3028–3035, 2022, doi: 10.1016/j.matpr.2020.10.238.

[14] X. Chen, L. Liu, P. Y. Yu, and S. S. Mao, "Increasing solar absorption for photocatalysis with black hydrogenated titanium dioxide nanocrystals," *Science*, vol. 331, pp. 746–750, 2011, doi: 10.1126/science.1200448.

[15] Y. Liu et al., "Synthesis of Cu, N-doped TiO_2 nanotube and study on photoelectric properties," *Pre-Print*, 2018, doi: 10.20944/preprints201808.0203.v1.

[16] K. Siwińska-Stefańska et al., "TiO_2-ZnO binary oxide systems: Comprehensive characterization and tests of photocatalytic activity," *Materials*, vol. 11, p. 841, 2018, doi: 10.3390/ma11050841.

[17] A. Mazabuel-Collazos and J. E. Rodríguez-Páez, "Chemical synthesis and characterization of ZnO–TiO_2 semiconductor nanocomposites: Tentative mechanism of particle formation," *Journal of Inorganic and Organometallic Polymers and Materials*, vol. 28, pp. 1739–1752, 2018, doi: 10.1007/s10904-018-0827-6.

[18] A. Toghan, A. Modwi, M. Khairy, and K. K. Taha, "Influence of TiO2 concentration on the characteristics of ZnO nanoparticles fabricated via sonication assisted with gelatin," *Chemical Physics*, vol. 551, p. 111350, 2021, doi: 10.1016/j.chemphys.2021.111350.

[19] M. B. A. Taee and B. M. A. Shabander, "Study the Effect of ZnO Concentrations on The Photocatalytic Activity of TiO_2/Cement Nanocomposites," *Chemistry Methodology*, vol. 6, no. 11, pp. 831–841, 2022, doi: 10.22034/chemm.2022.352379.1578.

[20] P. M. Smijs and S. Pavel, "Titanium dioxide and zinc oxide nanoparticles in sunscreens: Focus on UV attenuation," *Advances in Colloid and Interface Science*, vol. 123–126, pp. 31–40, 2011.

[21] L. M. Santos et al., "Structural characterization of Ag-doped TiO_2 with enhanced photocatalytic activity," *RSC Advances*, vol. 5, no. 125, pp. 103752–103759, 2015, doi: 10.1039/C5RA19309K

[22] N. Mokrani, E. G. Temam, H. B. Temam, H. Barkat, and M. Althamthami, "Enhancing water purification with light-activated strontium-doped ZnO thin films," *Advances in Natural Sciences: Nanoscience and Nanotechnology*, vol. 16, no. 1, p. 015012, 2025, doi: 10.1088/2043-6262/ada005.

[23] E. G. Temam, F. Djani, S. Rahmane, H. B. Temam, and B. Gasmi, "Photocatalytic activity of Al/Ni doped TiO_2 films synthesized by sol-gel method: dependence on thickness and crystal growth of photocatalysts," *Surfaces and Interfaces*, vol. 31, p. 102077, 2022, doi: 10.1016/j.surfin.2022.102077.

[24] M. Grätzel, B. O'Regan, and D. Fitzmaurice, "Structural and optical studies of TiO_2:Ag_2O nanocomposites by sol-gel method," *Journal of Materials Chemistry*, vol. 1, pp. 547–558, 1991.

[25] X. Jaramillo-Fierro, S. González, H. A. Jaramillo, and F. Medina, "Synthesis of the $ZnTiO_3$/TiO_2 nanocomposite supported in ecuadorian clays for the adsorption and photocatalytic removal of methylene blue dye," *Nanomaterials (Basel)*, vol. 10, no. 9, p. 1891, doi: 10.3390/nano10091891.

[26] C. Byrne, R. Fagan, S. Hinder, D. E. McCormack, and S. C. Pillai, "New approach of modifying the anatase to rutile transition temperature in TiO_2 photocatalysts," *RSC Advances*, vol. 6, no. 97, pp. 95232–95238, 2016, doi: 10.1039/C6RA19759K.

[27] E. A. Reynoso-Soto et al., "Photocatalytic degradation of nitrobenzene using nanocrystalline TiO_2 photocatalyst doped with Zn ions," *Journal of the Mexican Chemical Society*, vol. 57, no. 4, pp. 298–305, 2013.

[28] M. Kumar, S. Sheoran, and S. Bhattacharya, "Exploring chalcohalide perovskite-inspired materials ($Sn_2SbX_2I_3$; X = S or Se) for optoelectronic and spintronic applications," *Journal of Physical Chemistry Letters*, vol. 14, no. 45, pp. 10158–10165, 2023, doi: 10.1021/acs.jpclett.3c02475.

[29] D. Ramírez-Ortega, A. M. Meléndez, P. Acevedo-Peña, I. González, and R. Arroyo, "Semiconducting properties of ZnO/TiO_2 composites by electrochemical measurements and their relationship with photocatalytic activity," *Electrochimica Acta*, vol. 140, pp. 541–549, 2014, doi: 10.1016/j.electacta.2014. 06.060.

[30] R. Mohamed et al., "Facile synthesis of mesoporous Ag_2O–ZnO heterojunctions for efficient promotion of visible light photodegradation of tetracycline," *ACS Omega*, vol. 5, no. 51, pp. 33269–33279, 2020, doi: 10.1021/acsomega.0c 04969.

[31] N. A. Erfan, M. S. Mahmoud, H. Y. Kim, and N. A. Barakat, "Synergistic doping with Ag, CdO, and ZnO to overcome electron-hole recombination in TiO_2 photocatalysis for effective water photo splitting reaction," *Frontiers in Chemistry*, vol. 11, p. 1301172, 2023, doi: 10.3389/fchem.2023.1301172.

[32] P. Yang et al., "Ball-milling of titanium dioxide and zinc oxide for enhanced UV protection," *Frontiers in Materials*, vol. 10, p. 1273659, 2023, doi: 10.3389/fmats.2023.1273659.

[33] M. Adzis, I. R. Shah, K. Saeed, and S. Abdullah, "Modification of silver oxide/silver doped titanium dioxide (Ag_2O/Ag-TiO_2) photocatalyst using an immobilized reverse photocatalytic reactor (IPR)," *Materials*, vol. 16, no. 5, p. 1805, 2023, doi: 10.3390/ma16051805.

[34] G. G. Riungu, S. W. Mugo, J. M. Ngaruiya, G. M. John, and N. Mugambi, "Optical band energy, Urbach energy and associated band tails of nano crystalline TiO_2 films at different

annealing rates," *American Journal of Nanosciences*, vol. 7, no. 1, pp. 28–34, 2021.

[35] A. Naldoni et al., "Effect of nature and location of defects on bandgap narrowing in black TiO_2 nanoparticles," *Journal of the American Chemical Society*, vol. 134, no. 18, pp. 7600–7603, 2012.

[36] H. Nezzal et al., "Photo-deposition of AgO thin films on TiO_2 substrate for (PN) hetero-junction applications: Considering the degree of contamination," *Journal of Alloys and Compounds*, vol. 1010, p. 177331, 2025.

[37] N. Mokrani et al., "Boosting photocatalytic stability: hydrophilic Sr-doped ZnO thin films prepared via the SILAR method for enhanced performance over multiple cycles," *Physica Scripta*, vol. 99, no. 9, p. 0959a4, 2024.

[38] N. A. Mohamed, T. K. Ibrahim, and H. M. Ibrahim, "UV protection and antibacterial activities of ZnO/TiO_2 nanocomposites," *Materials Chemistry and Physics*, vol. 242, p. 122642, 2020, doi: 10.1016/j.matchemphys.2019.122642.

[39] M. Baalousha, A. M. Pyle, and A. Lead, "An overview of the environmental fate and toxicity of titanium dioxide nanoparticles," *Science of The Total Environment*, vol. 717, p. 137212, 2020, doi: 10.1016/j.scitotenv.2020.137212.

[40] J. Ye, Z. Qian, H. Li, and X. Jiang, "Photocatalytic performance of anatase TiO_2 with surface modifications," *Catalysis Today*, vol. 231, pp. 120–130, 2014.

[41] Z. Li, J. Shen, and X. Li, "Synergistic effect of ZnO and TiO_2 in enhancing photocatalytic properties," *Applied Surface Science*, vol. 487, pp. 634–642, 2019.

[42] Y. Wu et al., "Enhanced visible light photocatalytic activity of ZnO/TiO_2 heterojunction nanocomposites," *Journal of Alloys and Compounds*, vol. 790, pp. 552–559, 2019.

[43] M. Zhang, Y. Yu, and H. Wang, "Photoelectrochemical properties of TiO_2/ZnO composites for water splitting," *Journal of Materials Science: Materials in Electronics*, vol. 30, no. 24, pp. 22116–22124, 2019.

[44] S. Li et al., "Band structure engineering of TiO_2-based photocatalysts for enhanced visible light activity," *Applied Catalysis B: Environmental*, vol. 238, pp. 1–9, 2018.

[45] A. Kumar, S. K. Sharma, and M. Kumar, "Recent advances in TiO_2-ZnO composites for photocatalytic applications," *Materials Today Chemistry*, vol. 14, p. 100198, 2019.

[46] H. Zhao, Z. Liu, and W. Li, "Synthesis and photocatalytic activities of ZnO/TiO_2 heterojunction nanostructures," *Journal of Photochemistry and Photobiology A: Chemistry*, vol. 370, pp. 80–88, 2019.

[47] R. Sharma, A. D. Yadav, and P. Kumar, "Visible light-driven photocatalytic degradation of pollutants using ZnO/TiO_2 composites," *Environmental Science and Pollution Research*, vol. 27, pp. 12256–12268, 2020.